Development of Lumbar Spine Injury Risk Function for 50th Percentile THUMS v4.1 VW Group Male Model

Priti Yadav, Fenna Neumann, Debasis Sahoo

Abstract This study aimed to develop lumbar spine injury risk curves for the THUMS v4.1 VW Group human body model, using tissue-level strain and stress-based metrics, and to evaluate their predictive performance to identify the most reliable injury criterion. Numerical simulations replicating a wide range of full-body and lumbar-segment experimental loading conditions were conducted, and tissue responses, including maximum principal strain and von Mises strain of cortical and trabecular bone, trabecular pressure, and trabecular peak virtual power, were computed. Survival analysis was performed to construct the injury risk curves, which were compared using area under the curve, Akaike information criterion, log-likelihood, and normalised confidence interval size at 50% injury risk. Among all evaluated metrics, trabecular peak virtual power showed the strongest predictive capability, with the most favourable statistical fit and discrimination. Cortical strain measures also performed robustly and provided consistent predictions across loading conditions. Trabecular pressure demonstrated intermediate predictive strength, while trabecular strain-based criteria showed reduced performance. Validation using independent fracture cases confirmed that peak virtual power and cortical strain metrics reliably identified injury outcomes. The resulting injury risk curves provide a model-specific, tissue-level basis for lumbar spine injury assessment in virtual automotive safety evaluation.

Keywords HBM, Lumbar spine, Pressure, Peak virtual power, Strain.

I. INTRODUCTION

Lumbar spine injuries remain a significant safety concern in road traffic accidents despite continuous advances in vehicle crashworthiness and restraint systems [1-2]. Although modern safety technologies have substantially reduced fatal trauma, survivable crashes continue to produce musculoskeletal injuries, including those affecting the thoracic and lumbar spine [1]. Epidemiological studies consistently identify motor vehicle collisions (MVCs) as a major contributor to thoracolumbar spine trauma, accounting for approximately 25–50% of reported spinal injuries in developed countries [3]. Frontal impacts are most frequently associated with lumbar vertebral fractures in restrained occupants [1]. Recent work has further indicated that lumbar injury risk may be exacerbated in reclined seating configurations [4], which are expected to become increasingly common in future vehicle interiors. Increased seat-back recline alters occupant posture and modulates the load path through the spine, potentially increasing axial loading of the lumbar vertebrae [5]. Consequently, lumbar injury assessment remains relevant for both conventional seating and emerging mobility concepts. In this context, understanding the anatomical distribution of injuries is essential.

Vertebral fractures are concentrated at the thoracolumbar junction, with a substantial proportion occurring between T10 and L2 [6]. Among these, L1 is most frequently fractured, followed by T12 and L5, whereas L2 and L3 injuries are less common [1]. This distribution is generally attributed to the anatomical transition from the relatively stiff, rib-supported thoracic spine to the more flexible lumbar spine, which leads to increased mechanical demand at the junction during dynamic loading [7]. Compression and anterior wedge fractures are the most reported injury types, with burst fractures observed at higher loading severities [1,3]. These injuries, typically classified as AIS2+ or higher, are associated with prolonged recovery periods, functional impairment, and significant healthcare and socioeconomic burden [3]. A detailed understanding of lumbar spine injury mechanisms is therefore essential to support improvements in automotive safety design. Lumbar trauma in frontal crashes results from complex interactions among occupant motion, seat-belt restraint forces, pelvis kinematics, and upper torso rotation.

Experimental studies using post-mortem human subjects (PMHS) have demonstrated that combined axial

P. Yadav (e-mail: priti.yadav@vaiva.io) is an Engineer at VAIVA GmbH in Gaimersheim, Germany. F. Neumann is a PhD student at Volkswagen AG in Wolfsburg and University of Munich, Germany. D. Sahoo is a Senior Biomechanical Engineer at Volkswagen AG in Wolfsburg, Germany.

compression and flexion bending is the predominant loading mechanism leading to lumbar vertebral body fracture under frontal impact conditions [8-9]. These experiments established tolerance characteristics of the lumbar spine under loading conditions representative of automotive environments, and subsequent studies further emphasised the influence of loading rate, occupant posture, and boundary conditions on injury response [10-12].

Finite element (FE) human body models (HBMs) have increasingly been adopted to investigate spinal injury mechanisms under realistic crash scenarios. These models offer detailed anatomical representation and enable quantification of local mechanical variables, such as stress and strain within vertebral structures, which is difficult to measure experimentally. As a result, HBMs have become widely applied in vehicle safety development and are expected to play a central role in future virtual assessment procedures, supported by initiatives such as HBM4VT and Euro NCAP CP550 [13-14].

The availability of local tissue-level response from HBMs has enabled lumbar spine injury assessment using simulation-derived mechanical variables in addition to external loading measures. However, the published HBM-based lumbar injury literature is still limited. Tushak *et al.* [15] developed a GHBMC-M50-specific lumbar fracture injury risk curve (IRC) from simulated compression-flexion loading and evaluated both a structural metric and local material-response measures, with cortical-bone shell von Mises stress emerging as the most promising local predictor. Iraeus *et al*. [16] also developed a tissue-based IRC for lumbar compression fractures based on trabecular bone compressive strain. In addition, Rieger *et al*. [17] showed that pressure distributions within the vertebrae were associated with fracture location under dynamic loading, supporting pressure-related response as a relevant candidate indicator for lumbar injury risk assessment. In addition to commonly used stress- and strain-based predictors, peak virtual power (PVP), a thermodynamically motivated metric derived from the Clausius–Duhem inequality and previously applied to brain injury prediction [18] may also be relevant for vertebral fracture assessment. PVP represents the peak irreversible work rate within the material and is defined as:

$$PVP = max\left(\sum_{ij} \sigma_{ij}(t)\dot{\varepsilon}_{ij}(t)\right) \tag{1}$$

where $\sigma_{ij}(t)$ and $\dot{\varepsilon}_{ij}(t)$ are the components of the stress and strain rate tensors, respectively. This explicit summation form represents the scalar product of the tensors. PVP is defined as the maximum value of this scalar over time during the loading history.

Published HBM studies demonstrate that local tissue-level metrics can be effective for predicting lumbar vertebral injury risk. However, these studies use different injury metrics, HBMs and loading conditions, making direct comparison difficult. As a result, it remains unclear which metric provides the most reliable and practically relevant predictor for a given HBM. A systematic evaluation of multiple metrics within a consistent modelling framework is therefore needed to identify predictors that are both biomechanically meaningful and practically applicable.

Accordingly, the objective of the present study was to develop lumbar spine IRCs for the 50th percentile THUMS v4.1 VW group HBM (VWG-HBM) using a broad combined dataset of full-body and isolated lumbar reconstructions, and to compare several tissue-level mechanical metrics in order to determine the most reliable injury predictor for lumbar vertebral fracture in this model configuration.

II. METHODS

A multi-stage methodology was applied to develop lumbar spine IRCs for the VWG-HBM. First, a broad set of PMHS experiments representing full-body and isolated lumbar spine loading conditions were reconstructed using FE simulations. In total, 122 data points were included in the analysis. Second, local tissue-level mechanical response metrics were extracted from vertebrae T12–L5. Third, survival-based statistical modelling was used to correlate these metrics to experimentally reported injury outcomes. Finally, the predictive performance of the evaluated tissue-level metrics was compared to identify the most reliable injury indicator within the 50th percentile male VWG-HBM framework.

Experimental Database

The PMHS experiments considered for this study include both full-body and isolated lumbar spine experiments to cover a broad range of lumbar loading environments encountered in current and anticipated future seating postures. Full-body tests included frontal and rearward sled experiments [19-21], reclined and oblique loading

[21-23], under-body blast loading [24-25], loading during posterior landing of astronauts [26], and loading representing inverted impacts [27-29]. Across these studies the reconstructed fully-body loading conditions covered frontal sled velocities ranging from approximately 30–50 km/h, oblique sled test at 30 km/h, reclined frontal sled tests at 32–33 km/h, and vertical or inferior-superior impact velocities between 2.8 m/s and 6.1 m/s. Additional loading exposure included test conditions characterised by 4–8 m/s pulse inputs with time-to-peak values between 5 ms and 10 ms, and targeted acceleration of 10 g and 20 g.

The database also incorporated detailed isolated lumbar spine segment tests, which provide precise vertebral injury outcomes under controlled loading. These included high and low compression tests on different lumbar segments with compression velocities of 0.5 m/s or 1.0 m/s [30-31], dynamic loading and ejection simulations [32-33], and combined compression-flexion experiments with compression force of 2200–4500 N and flexion rate of approximately 600°/s [34].

All considered experimental load cases, including subject anthropometry, specific loading condition and AIS2+ injury outcomes, are summarised in Table AI in the Appendix.

Numerical Modelling of Experiments

For the present study, the 50th percentile male occupant VWG-HBM [35-37] was used. The model is based on the THUMS v4.1 occupant model developed by Toyota (Toyota Motor Corporation, Toyota, Japan) and was translated to VPS (ESI Group, Keysight, Bagneux, France). It has been further modified by the Volkswagen Group to improve biofidelity and numerical robustness under diverse automotive loading conditions. The model has been certified under Euro NCAP CP550 Qualification Procedure for HBMs. In addition, the pedestrian variant of this model has been certified under the Euro NCAP TB024 Pedestrian HBM Certification protocol [38].

In the lumbar spine, the cortical thickness of the posterior regions of the vertebrae was modified relative to the baseline THUMS v4.1 model based on literature data [39]. As a result, the cortical thickness for vertebrae T12 to L5 ranges from 0.51 to 1.21 mm (see Fig. A1 in Appendix). The material models and element formulations for both cortical and trabecular bone remain identical to those in the original THUMS v4.1 model, employing elastic–plastic behavior with fully integrated elements.

Each experimental test was reconstructed using the 50th percentile male VWG-HBM by reproducing the PMHS initial posture, the experiment-specific support and fixation conditions, and the corresponding loading characteristics. Numerical simulations were performed using the PAM-CRASH 2023 solver (ESI Group, Keysight, Bagneux, France). In the full-body reconstructions, seat-belt routing, seat geometry, padding, and impactor configurations were modelled according to the original test descriptions. For isolated lumbar-segment experiments, the boundary conditions were defined to replicate the constraints and applied load paths of the cadaveric specimens. All input parameters, including sled pulses, impact velocities, displacements, and segment-level loading conditions were implemented following the details reported in the source publications (summarised in Table AI in Appendix).

Model responses were assessed for biomechanical plausibility through comparison of simulated kinematic and kinetic responses with available PMHS data. Validation results for various loading cases are provided in the Appendix (Fig. A2–A6), demonstrating the model's ability to reproduce key response characteristics across different loading conditions. Results are shown for load cases with publicly available experimental data or corridors, and they illustrate the model behaviour for the corresponding loading modes.

Following verification of consistent model behaviour, tissue-level injury metrics were extracted for cortical and trabecular bone in vertebrae T12–L5 using Visual Viewer (ESI Group, Keysight, Bagneux, France). For shell elements, stress and strain tensor components were extracted from the outermost layers (top and bottom integration points) of a through-thickness discretization comprising five integration points, without thickness averaging. The reported metrics correspond to the maximum response observed across these layers and over time. Extracted metrics included maximum principal strain (MPS), von Mises strain (cortical and trabecular), trabecular pressure, and trabecular PVP.

All injury metrics were obtained directly from the finite element solver outputs, except for PVP. In the present study, to account for the complete rate-dependent energy transfer within the vertebra, PVP was computed according to Eq. (1), using the Cauchy stress tensor $\sigma_{ij}(t)$ and the total strain-rate tensor $\dot{\varepsilon}_{ij}(t)$. Stress and strain tensors were exported over time for each element, and the strain rate was obtained by differentiating the strain time histories. The use of total strain-rate tensor as dimensionally equivalent proxy ensures that the entire power history of the dynamic loading is captured.

PVP was evaluated only for trabecular bone, as it represents a volumetric measure of the rate of mechanical work that is most appropriately applied to 3D continuum elements. Cortical bone, however, is modeled using shell elements, for which volume-based power density is not directly applicable. Therefore, only strain-based metrics were used to characterize cortical bone response.

For all metrics, the maximum value across all elements and simulation time was first identified for each vertebra. To mitigate numerical artifacts, the upper 1% of elements was excluded based on the maximum values observed across all elements and over the entire simulation time for each vertebra. The remaining maximum value for each vertebra was retained, and the largest value among T12–L5 was taken as the representative response metric for the corresponding test case.

Statistical Modelling of IRC Generation

Injury outcomes were taken directly from the PMHS studies. Tests reporting AIS2+ vertebral fractures were classified as injury cases, and tests without such fractures were classified as non-injury cases. The statistical modelling applied censoring according to the available information: injury cases were treated as left-censored, non-injury cases as right-censored, and one test from [26] was treated as interval-censored because the fracture occurred between two documented loading levels.

The relationship between tissue-level metrics and fracture occurrence was evaluated using Weibull, log-normal, and log-logistic survival distributions. Model performance was assessed using the area under the curve (AUC), the Akaike Information Criterion (AIC), log-likelihood values, and the normalised confidence-interval size at 50% injury risk ($NCIS_{50}$). All analyses were performed in R. The metric demonstrating the most favourable overall performance was selected for constructing the lumbar spine IRCs for the VWG-HBM.

For comparative assessment and external consistency checking, the PMHS data from [40] were used, as this study provided male T12–L5 lumbar spine specimens with well-defined axial-acceleration loading inputs and clearly reported injury outcomes. In this work, only the male specimens subjected to a single dynamic test exposure were included.

Experimental outcomes are binary (injury/no injury), whereas model outputs are continuous predicted probabilities derived from survival analysis. Thus, no fixed threshold (e.g., 50% or 90%) is applied; 50% represents the median injury tolerance, and higher probabilities indicate increasing injury risk.

III. RESULTS

Six candidate tissue-level metrics were evaluated: trabecular von Mises strain, trabecular MPS, trabecular pressure, trabecular PVP, cortical von Mises strain, and cortical MPS. Among Weibull, log-normal, and log-logistic distributions, the Weibull distribution provided the best fit for all six criteria based on the lowest AIC values. The fitted parameters and statistical performance measures are summarised in Table I, and the corresponding IRCs with confidence intervals are shown in Fig. 1.

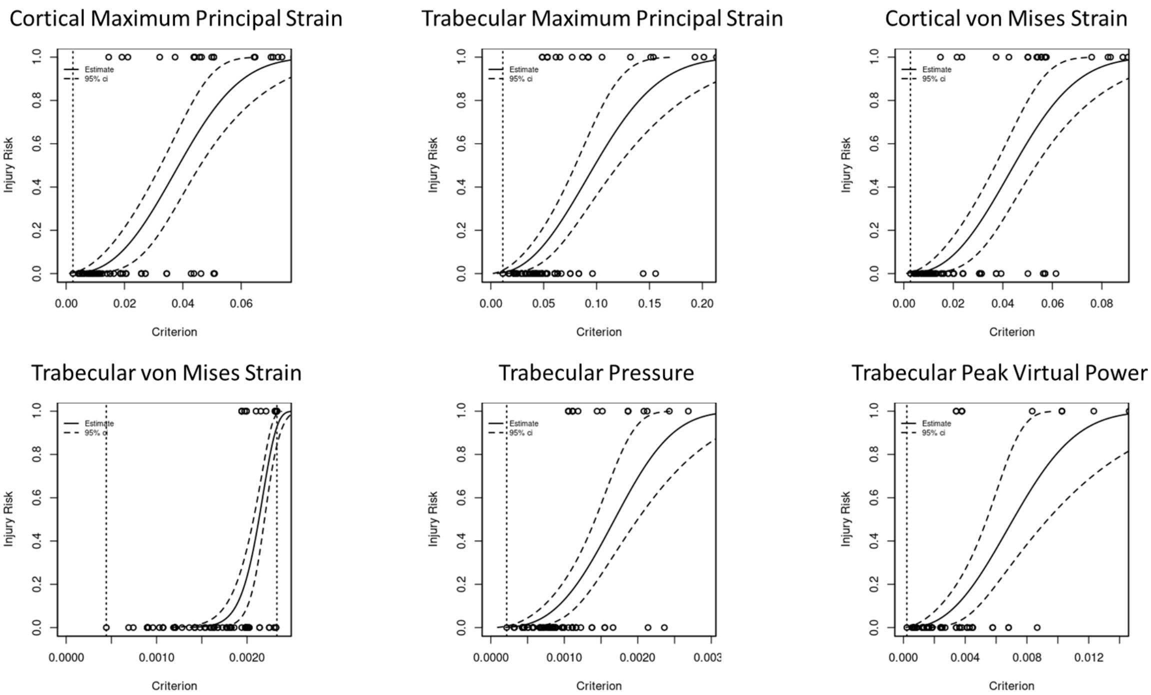

Fig. 1. Injury risk curves derived from multiple tissue-level metrics. The plot shows the mean curve and 95% confidence intervals. The ordinate represents the probability of AIS2+ lumbar spine injury, while the abscissa denotes the corresponding magnitude of the injury criterion. Strain-based metrics (cortical and trabecular maximum principal strain, and von Mises strain) are dimensionless (mm/mm). Trabecular pressure is expressed in [GPa], and trabecular peak virtual power (PVP) is expressed in [GPa/ms]. The specific criterion associated with each risk curve is indicated above its respective plot.

Across all considered metrics, trabecular PVP demonstrated the strongest overall performance. It achieved the highest AUC (0.9568), the lowest AIC (40.71), the lowest BIC (46.31), and the highest log-likelihood (-18.35), indicating superior discrimination and model fit relative to all other criteria. Its $NCIS_{50}$ value of 0.56 indicated a moderate but acceptable uncertainty band for a biologically variable fracture outcome.

The cortical strain metrics ranked next in performance. Cortical von Mises strain and cortical MPS both achieved AUC values of 0.9504. Their AIC values (53.48 and 54.48, respectively) placed them second to PVP. Their $NCIS_{50}$ values of 0.37 and 0.35, respectively, indicated tighter confidence intervals than PVP and comparatively stable tolerance predictions.

Among the trabecular metrics, pressure performed well, with AUC = 0.9498 and AIC = 59.72, but remained inferior to PVP and the cortical strain-based criteria. Trabecular MPS showed reduced performance, with a lower AUC and wider uncertainty band. The weakest criterion was trabecular von Mises strain, which showed an unrealistically steep Weibull shape factor, suggesting poor physiological plausibility despite nominal discrimination.

TABLE I

50% RISK TOLERANCE LIMIT AND PERFORMANCE METRICS FOR EACH EVALUATED INJURY CRITERION

Criterion	Metric value at 50% Injury Probability	Performance Metrics			
		AUC	AIC	Loglik	$NCIS_{50}$
Cortical MPS (mm/mm)	0.0386	0.95038	54.4837	-25.2419	0.352332
Trabecular MPS (mm/mm)	0.0982	0.94451	65.8749	-30.9735	0.414460
Cortical von Mises Strain (mm/mm)	0.0445	0.95038	53.4779	-24.739	0.370786
Trabecular von Mises Strain (mm/mm)	0.0021	0.94199	67.4669	-31.7335	0.047619
Trabecular Pressure (GPa)	0.0017	0.94982	59.718	-27.859	0.352941

Trabecular PVP(GPa/ms)	0.0071	0.95681	40.7059	-18.353	0.563380

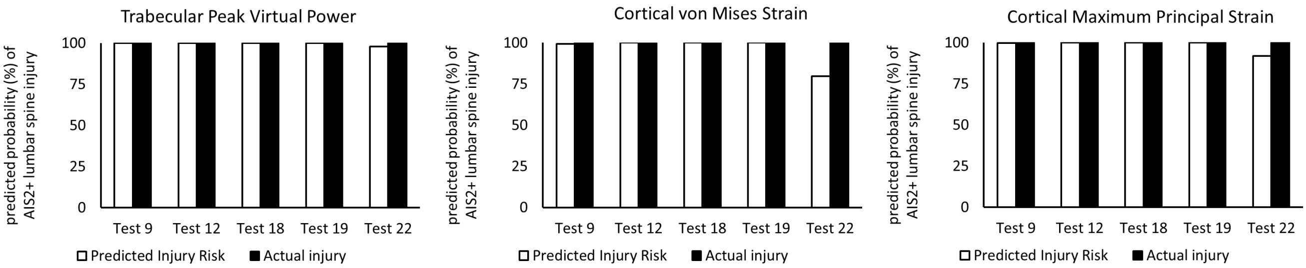

Fig. 2. Predicted injury probabilities versus observed outcomes for five fracture cases from [40], shown for trabecular PVP, cortical von Mises strain, and cortical MPS. The ordinate represents the predicted probability of AIS2+ lumbar spine injury derived from the corresponding injury risk curves.

Comparative assessment using PMHS fracture cases from Stemper *et al.* [40] showed that all three evaluated criteria; trabecular PVP, cortical von Mises strain, and cortical MPS provided consistently high injury predictions across all five fracture cases (see Fig. 2). Each criterion correctly identified all cases as high-risk, with predicted injury probabilities generally exceeding 90%. Minor variability was observed only in the lowest-severity case (Case 22), where cortical von Mises strain predicted a lower, yet still elevated, risk. Overall, these findings indicate that all three criteria exhibit strong external validity when applied to the 50th percentile male occupant VWG-HBM and are capable of reliably identifying vertebral fracture across independent loading conditions.

IV. DISCUSSION

This study evaluated six tissue-level metrics for predicting lumbar vertebral injury in the 50th percentile male occupant VWG-HBM using a consistently reconstructed set of PMHS tests and a uniform statistical and injury-classification approach. Among the evaluated metrics, trabecular PVP, cortical MPS, and cortical von Mises strain demonstrated the most stable and reliable performance across statistical indicators and comparative assessment using independent PMHS cases. These findings highlight the value of trabecular PVP as a rate-sensitive indicator reflecting internal energy transfer mechanisms governing vertebral failure under crash loading.

The strong predictive capability of PVP is consistent with established findings that vertebral failure is influenced by loading magnitude and loading rate [12]. PVP inherently incorporates strain-rate effects through the stress–strain-rate interaction, enabling it to capture the rate of internal energy transfer during deformation. Under dynamic loading conditions typical in crash environments, rapid energy transfer plays a critical role in structural failure.

In the VWG-HBM, trabecular bone is modelled using an elastic-plastic formulation without explicit rate dependency. However, PVP introduces rate sensitivity at the response level through the inclusion of strain-rate. Higher loading rates generate increased strain rates, resulting in elevated rates of mechanical work. Thus, the observed rate sensitivity arises from the kinematics of deformation, rather than from intrinsic rate-dependent material behaviour. This kinematic effect likely explains the superior statistical performance of PVP across AUC, AIC/BIC, and log-likelihood metrics.

In this study, PVP is computed using the total strain-rate tensor, meaning it represents the peak internal power density including both recoverable and dissipative components. While this provides a robust and consistent measure of dynamic mechanical response, using plastic strain-rate instead would result irreversible energy dissipation and reduce the absolute magnitude of PVP. Although this is not expected to significantly alter injury predictability trends, it warrants further investigation. Future work should evaluate the sensitivity of PVP to strain-rate definitions and explore methods for extracting plastic strain-rate tensor from FE solvers, which is currently not supported in the VPS solver.

In addition to PVP, strain-based metrics in the cortical bone demonstrated strong predictive capability and clear biomechanical relevance. The cortical shell and endplate regions play central roles in vertebral strength and fracture initiation [41-42], providing a strong mechanistic foundation for strain-based metrics. MPS reflects local tensile failure modes, whereas von Mises strain captures multiaxial deformation in a single scalar value. Their similar ranking suggests that either can serve as a practical and robust injury indicator, especially when ease of computation or interpretability is prioritised over rate sensitivity.

Among the trabecular-based metrics, pressure demonstrated moderate predictive performance, reflecting its ability to capture compressive load transfer through the cancellous core [43]. While axial compression dominates many experimental configurations, real-world vertebral injuries often involve combined loading (compression, bending, and shear), which increases the contribution of cortical failure mechanisms [34,44–46]. As pressure is limited to compressive response, it cannot fully represent these interactions.

The comparatively weaker performance of trabecular strain-based metrics aligns with previous observations that vertebral failure under dynamic conditions results from interactions among trabecular collapse, cortical shell engagement, and endplate deformation rather than trabecular strain in isolation [44-46]. The steep Weibull slope for trabecular von Mises strain further questions its physiological plausibility, as human vertebral tolerance exhibits broad variability influenced by factors such as age, bone quality, spinal level, and loading mode [47-50]. A key contributing factor is the dependence of strain-based metrics on local material representation. In the present HBM, trabecular bone is modelled as a continuum elastic–plastic material, which does not explicitly resolve microstructural damage processes. As a result, local strain measures are sensitive to modelling assumptions and may not fully capture the underlying failure mechanisms. In contrast, energy-based measures such as PVP reflect the overall intensity of mechanical response, making them less dependent on local representation and better suited to capturing global failure behaviour. Although this modelling simplification is common across current HBMs, it limits the ability of trabecular-based metrics to provide a direct interpretation of vertebral failure. Consequently, their predictive capability remains lower than that of cortical strain-based criteria, which are more directly associated with fracture-relevant deformation patterns.

Overall, the findings are consistent with previous HBM and FE studies showing the relevance of tissue-level injury metrics [15-17], while extending this understanding by demonstrating that, within the VWG-HBM, a rate-sensitive parameter such as PVP can outperform strain-only predictors when a broad range of dynamic conditions is considered. This aligns with evidence that lumbar injury mechanisms depend strongly on loading rate, posture, and combined loading modes [12][34].

The GHBMC model [14] evaluated tissue-level predictors under combined compression–flexion loading and found cortical von Mises stress to be the most effective criterion for fracture prediction in those conditions. The VIVA+ lumbar spine model, [15] focused on compression-dominated loading, and developed an injury risk function based on trabecular compressive strain in the superior–inferior direction to predict endplate-related compression fractures. The present study aligns with these observations while highlighting model-specific sensitivities. Cortical von Mises strain also performed well in the VWG-HBM, serving as a consistent secondary predictor alongside PVP. Unlike the VIVA+ work, which used a compression-specific trabecular strain measure, the current study evaluated trabecular MPS. These distinctions help explain differences in trabecular strain performance across models: the optimal tissue-level metric depends on each HBM's structural design and the dominant loading modes used in IRC development database. Despite these variations, the overall evidence supports the robustness of cortical strain-based criteria and the value of rate-sensitive metrics such as PVP for lumbar injury assessment across diverse loading scenarios.

These insights are particularly relevant for emerging reclined seating configurations, where changes in seat-back angle modify occupant posture and load paths through the lumbar spine, increasing axial alignment and altering vertebral loading patterns [11]. Such variations can lead to differences in the relative contribution of compression, bending, and shear components to the overall response. In this context, metrics that remain stable across varying loading conditions and response histories, such as PVP, may offer advantages in terms of robustness. This does not imply that different injury criteria are required for different configurations; rather, it highlights the importance of selecting metrics that can consistently represent injury-related responses under diverse loading scenarios. In the present study, cortical strain-based measures also demonstrated strong performance and remain practical alternatives due to their clear anatomical interpretation and computational efficiency.

Comparison of structural tolerance data supports the plausibility of the selected criteria. Lumbar vertebral compressive failure thresholds span a wide range (0.6–15.6 kN) [47], and injury metrics that produce gradual risk transitions, such as PVP and cortical strain measures, are therefore more consistent with known variability. In contrast, the abrupt risk transition predicted by trabecular von Mises strain appears less physiologically realistic. As tissue-level predictors, PVP and cortical strain criteria are not expected to map directly to whole-vertebra force levels, but instead serve to capture internal mechanical states associated with fracture.

A key strength of this study is the inclusion of diverse loading environments representative of crash-relevant conditions. In addition, multiple tissue-level predictors were evaluated within a single HBM framework, eliminating inter-model variability and enabling direct comparison of their predictive capability.

Direct comparison with previously published injury criteria was not performed in the present study. This is primarily due to the model-specific nature of many established criteria, which are often calibrated and validated for a particular HBM framework. Previous research has demonstrated that injury metrics, particularly kinematic- and tissue-based criteria, may require recalibration when transferred between different HBMs due to variations in geometry, material modelling, and structural response characteristics [15].

As a result, applying existing criteria directly to the VWG-HBM without appropriate re-calibration may lead to misleading conclusions regarding predictive performance. Instead, the current study focuses on the relative comparison of multiple candidate metrics within a consistent modelling framework, ensuring that the observed differences reflect their intrinsic predictive capability rather than inter-model variability. Future work could include cross-model validation or reparameterisation of established criteria to enable more direct comparisons.

There are some limitations to consider in this study. The representation of trabecular bone as a continuum elastic–plastic material without explicit strain-rate dependency may affect both the magnitude and spatial distribution of predicted responses. Although PVP partially accounts for rate effects through its formulation, incorporating rate-dependent material behaviour could further improve biofidelity.

Additionally, the representative response for each test case was defined as the maximum value across vertebrae T12–L5, reflecting a conservative injury assessment approach. This choice is based on the understanding that vertebral fracture is typically governed by the most critically loaded level rather than an average response across the segment. Due to variations in posture, boundary conditions, and load paths, peak responses may localise at different vertebral levels depending on the loading scenario. This approach is consistent with prior finite element-based lumbar spine injury studies, where tissue-level responses are reduced to peak scalar measures for correlation with injury outcomes [16]. However, this approach does not account for potential multi-level injury mechanisms or cumulative effects across adjacent vertebrae.

Another limitation relates to the representation of loading conditions, as the dataset used for IRC development comprises both full-body and segment-level simulations. While the full-body simulations capture combined loading conditions, a portion of the segment-level cases is predominantly compression-driven. Although the applied boundary conditions do not result in idealised pure compression at the vertebral level, the overall representation of flexion–compression and other combined loading modes remains limited. Since real-world lumbar spine injuries typically involve such combined loading scenarios, this may influence the relative performance of the evaluated injury metrics.

Furthermore, demographic variability, including age, sex, and bone mineral density, were not considered. Modelling simplifications such as mesh resolution and material homogenization may also reduce spatial variability and lead to poor injury prediction. A filtering approach was applied to exclude the upper 1% of element responses to reduce numerical artefacts and mesh-dependent outliers. While this improves robustness, absolute values may still be affected by modelling assumptions; however, the consistent framework allows for meaningful relative comparisons.

Finally, the derived injury risk curves are specific to the VWG-HBM and may not be directly transferable to other HBMs without recalibration, as injury criteria are known to be model-dependent. In addition, variability in PMHS datasets, including differences in test setups and injury reporting, introduces uncertainty. Tissue-level responses obtained from FE simulations cannot be directly validated and are influenced by modelling assumptions such as mesh density, material formulation, and element types.

Future work should focus on incorporating strain-rate dependent material properties, exploring alternative PVP formulations based on plastic strain rate, and developing combined injury metrics that integrate cortical and trabecular responses. Expanding datasets to better represent real-world loading conditions and subject variability would further improve robustness.

In summary, the current study supports the use of trabecular PVP as an effective rate-sensitive primary criterion for lumbar vertebral injury assessment in the VWG-HBM, with cortical MPS and cortical von Mises strain serving as strong, interpretable secondary criteria that may be more convenient to implement in post-processing workflows as they are usually supported in simulation software. These findings underscore the combined value of dynamic and deformation-based metrics and provide a solid foundation for future refinement and broader validation across different HBMs and emerging loading environments.

V. CONCLUSION

This study developed lumbar spine IRCs for the VWG-HBM using an extensive set of full-body and segment-level PMHS reconstructions and six tissue-level mechanical metrics. Trabecular PVP, cortical MPS, and cortical von Mises strain demonstrated the most consistent and reliable predictive performance, supported by statistical evaluation and independent validation. These metrics capture key aspects of deformation magnitude and loading rate relevant to vertebral failure and form a robust basis for HBM-specific lumbar injury assessment. The results provide an important foundation for virtual safety evaluation, particularly as future vehicle concepts introduce posture-dependent loading conditions, such as reclined seating. Future work should expand validation, explore hybrid metrics, and assess applicability across different HBMs.

VI. ACKNOWLEDGEMENTS

The authors would like to acknowledge Volkswagen AG for generously funding this study. The authors also thank Dr Giacomo Marini from AUDI AG for the financial support for the development of the initial simulation set-ups used in the lumbar spine validation work.

VII. REFERENCES

[1] Pintar, F. A., Yoganandan, N., Maiman, D. J., Scarboro, M., Rudd, R. W. (2012) Thoracolumbar spine fractures in frontal impact crashes. Annals of Advances in Automotive Medicine. Association for the Advancement of Automotive Medicine. Annual Scientific Conference, **56**: pp. 277–283.

[2] Rudd, R.W., Parenteau C.S. (2023) Serious spine injuries using 2017-2021 CISS and CIREN data effect of spinal degeneration comorbidities. Proceedings of the IRCOBI Conference, 2023, Cambridge, UK.

[3] Zileli, M., Sharif, S., Fornari, M. (2021) Incidence and Epidemiology of Thoracolumbar Spine Fractures: WFNS Spine Committee Recommendations. Neurospine, **18**(4): pp. 704–712.

[4] Richardson, R., Jayathirtha, M., et al. (2020). Thoracolumbar spine kinematics and injuries in frontal impacts with reclined occupants. Traffic Injury Prevention, **21**(sup1): pp. S66–S71.

[5] Su, Q., Zhang, Y., et al. (2019) 3D Computed Tomography Mapping of Thoracolumbar Vertebrae Fractures. Medical Science Monitor: International Medical Journal of Experimental and Clinical Research, **25**: pp. 2802–2810.

[6] Mataliotakis, G., Mohammad, S., Tsirikos, A. I. (2024) Injuries of the thoracic spine and thoracolumbar junction. Orthopaedics and Trauma, **38**(5): pp. 296–303.

[7] Rajasekaran, S., Kanna, R. M., Shetty, A. P. (2015) Management of thoracolumbar spine trauma: An overview. Indian Journal of Orthopaedics, **49**: pp. 72–82.

[8] Ortiz-Paparoni, M., Op 't Eynde, J., et al. (2021) The Human Lumbar Spine During High-Rate Under Seat Loading: A Combined Metric Injury Criteria. Annals of Biomedical Engineering, **49**(11): pp. 3018–3030.

[9] Adolph, T., Wisch, M., et al. (2013) Proceedings of the IRCOBI Conference, 2013, Cambridge, UK.

[10] Cutlan, R., Khokhar, M., et al. (2026) Lumbar Spine Orientation Affects Compressive Fracture Outcome. Annals of Biomedical Engineering, **54**(4): pp. 1076–1085. doi: 10.1007/s10439-024-03604-y. Epub 2024 Oct 25. PMID: 39453511; PMCID: PMC13035867.

[11] González-García, M., Weber, J., Peldschus, S., Eggers, A. (2026) Sensitivity of lumbar spine loadings to different seat characteristics and Human Body Model boundary conditions. Presented at: the IRCOBI Conference, 2026, Munich, Germany. [Under Review]

[12] Stemper, B. D., Yoganandan, N., et al. (2015) Rate-dependent fracture characteristics of lumbar vertebral bodies. Journal of the Mechanical Behaviour of Biomedical Matererials, **41**: pp. 271–279. doi: 10.1016/j.jmbbm.2014.07.035. Epub 2014 Aug 9. PMID: 25154535.

[13] HBM4VT Consortium (2021) Human Body Models for Virtual Testing. OpenVT Project Report, 2021.

[14] Euro NCAP CP550 (2023) Human Body Model Assessment Protocol.

[15] Tushak, S. K., Gepner, B. D., Pipkorn, B., Kerrigan, J.R. (2023) GHBMC-M50-specific Lumbar Spine Fracture Risk Prediction Considering Two Different Metrics. Proceedings of the IRCOBI Conference, 2023, Cambridge, UK.

[16] Iraeus, J., Poojary, Y. N., Jaber, L., John, J., Davidsson, J. (2023) A new open-source finite element lumbar spine model, its tuning and validation, and development of a tissue-based injury risk function for compression fractures. Proceedings of the IRCOBI Conference, 2023, Cambridge, UK.

[17] Rieger, L. K., Shah, A., et al. (2024) Subject-Specific Geometry of FE Lumbar Spine Models for the Replication of Fracture Locations Using Dynamic Drop Tests. Annals of Biomedical Engineering, **52**(4): pp. 816–831. doi: 10.1007/s10439-023-03402-y. Epub 2024 Feb 19. PMID: 38374520.

[18] Bastien, C., Neal-Sturgess, C., Davies, H., Cheng, X. (2020) Computing Brain White and Grey Matter Injury Severity in a Traumatic Fall. Mathematical and Computational Applications, **25**(3): p. 61.

[19] Shaw, G., Parent, D., et al. (2009) Impact response of restrained PMHS in frontal sled tests: skeletal deformation patterns under seat belt loading. Stapp Car Crash Journal, **53**: pp. 1–48. doi: 10.4271/2009-22-0001. PMID: 20058549.

[20] Acosta A.M., Ash J.H., et al. (2016) Comparison of whole body response in oblique and full frontal sled. Proceedings of the IRCOBI Conference, 2016, Malga, Spain.

[21] Uriot, J., Potier, P., Baudrit, P., et al. (2015) Reference PMHS Sled Tests to Assess Submarining. Stapp Car Crash Journal, 59: pp. 203–223. DOI: 10.4271/2015-22-0008. PMID: 26660745.

[22] NHTSA Reports (2012) Automated Vehicle Occupant Kinematics: (2021) Test ID 13119, 13109, and 12796. https://www.nhtsa.gov/research-data/research-testing-databases/#/vehicle.

[23] Richardson, R., Donlon, J., et al. (2021) Kinematic and Injury Response of Reclined PMHS in Frontal Impacts. SAE Technical Paper, 2020-22-0004, 2021, https://doi.org/10.4271/2020-22-0004.

[24] Dooley, C. J. (2016) Spinal Response and Injury Association from Whole Body PMHS in the Under Body Blast Loading Environment. Master Thesis: Johns Hopkins University, Baltimore, Maryland.

[25] Yoganandan, N., Moore, J., Arun, M. W., Pintar, F. A. (2014) Dynamic Responses of Intact Post Mortem Human Surrogates from Inferior-to-Superior Loading at the Pelvis. Stapp Car Crash Journal, 58: pp. 123–43. doi: 10.4271/2014-22-0005. PMID: 26192952.

[26] Bolte, J. H., Gustafson, H., Agnew, A. M., Kang, Y.-S. (2018) Injuries due to Lower Spine Blunt Force Impacts Associated with the Planetary Suit Body Seal Closure (BSC). Proceedings of the IRCOBI Conference, 2018, Athens, Greece.

[27] Roberts, C. W. & Kerrigan, J. R. (2015) Injuries and Kinematics: Response of the Cervical Spine in Inverted Impacts. 24th International Technical Conference on the Enhanced Safety of Vehicles (ESV), 2015, Gothenburg, Sweden.

[28] Kerrigan, J. R., Foster, J. B., et al. (2014) Axial Compression Injury Tolerance of the Cervical Spine: Initial Result. Short Communication. Traffic Injury Prevention, **15**, pp. S265-S269.

[29] Yoganandan, N., Sances, A. Jr, et al. (1986) Experimental spinal injuries with vertical impact. Spine (Phila Pa 1976), **11**(9): pp. 855–860. doi: 10.1097/00007632-198611000-00001. PMID: 3824059.

[30] Arun, M. W. J., Hadagali, P. et al. (2017) Biomechanics of Lumbar Motion-Segments in Dynamic Compression. Stapp Car Crash Journal, **61**: pp. 1–25. doi: 10.4271/2017-22-0001. PMID: 29394433.

[31] Duma, S. M., Kemper, A. R., McNeely, D. M., Brolinson, P. G., Matsuoka, F. (2006) Biomechanical response of the lumbar spine in dynamic compression. Biomedical Sciences Instrumentation, **42**: pp. 476–481. PMID: 16817654.

[32] Storvik, S. G. (2011) Development of an Experimental Model to Quantify Lumbar Spine Kinematics during Military Seat Ejection. Master's Thesis, Marquette University (http://epublications.marquette.edu/theses_open/110)

[33] Stemper, B. D., et al. (2012) Effect of Loading Rate on Injury Patterns During High Rate Vertical Acceleration. Proceedings of the IRCOBI Conference, 2012, Dublin, Ireland.

[34] Tushak, S. K., Donlon, J.P., et al. (2022) Failure tolerance of the human lumbar spine in dynamic combined compression and flexion loading. Journal of Biomechanics, **135**: 111051.

[35] Marini, G., Auriault, F., Junge, M., Sahoo, D. (2022) Methodology to account for cadaver versus living population effect in the development of human body model specific probabilistic rib injury criterion. Proceedings of the Fiftieth NHTSA Workshop on Human Subjects for Biomechanical Research, 2022

[36] Vieler, C., Marini, G., et al. (2024) Overview of Advancement and Application of HBMs in VW Group, 10th Symposium, Human Modeling and Simulation in Automotive Engineering.

[37] Sahoo, D., Jani, D., Marini, G. (2024) Validation THUMSv4.1 head model in Visual Performance Solution and development of model-specific head injury criteria: skull fracture, mild Diffuse Axonal injury and subdural haematoma. Proceedings of the IRCOBI Conference, 2024, Stockholm, Sweden.

[38] Jani, D., Staack, H., Teichmann, C. (2025) Integrated Head and Thorax Protection Evaluation for VRU Safety: A Simulation Based Approach, Proceedings of the IRCOBI Conference, 2025, Vilnius, Lithuania.

[39] Wagnac, E., Arnoux, P. J., Garo, A., El-Rich, M., Aubin, C. E. (2011) Calibration of hyperelastic material properties of the human lumbar intervertebral disc under fast dynamic compressive loads. Journal of Biomechanical Engineering, **133**(10): 101007. doi: 10.1115/1.4005224. PMID: 22070332.

[40] Stemper, B. D., Chirvi, S., et al. (2018). Biomechanical tolerance of whole lumbar spines in straightened posture subjected to axial acceleration. Journal of Orthopaedic Research: official publication of the Orthopaedic Research Society, **36**(6): pp. 1747–1756.

[41] Kopperdahl D.L., Morgan E.F., Keaveny T.M. (2002) Quantitative computed tomography estimates of the mechanical properties of human vertebral trabecular bone. Journal of Orthopaedic Research, 20(4): pp. 801–805.

[42] Fields, A. J., Liebenberg, E. C., Lotz, J. C. (2014) Innervation of pathologies in the lumbar vertebral end plate and intervertebral disc. The spine journal: official journal of the North American Spine Society, **14**(3): pp. 513–521. https://doi.org/10.1016/j.spinee.2013.06.075.

[43] Guerrero-Vargas, J. A., Sanchez-Quinones, P., et al. (2025) The Role of Trabecular, Ligamentous-Intervertebral Disk and Facet Joints Systems: A Finite Element Analysis in the L4-S1 Vertebrae. Global Spine Journal, 15(2): pp. 1212–1228. https://doi.org/10.1177/21925682241231525.

[44] Pachocki, L., Daszkiewicz, K., Łuczkiewicz, P., Witkowski, W. (2021) Biomechanics of Lumbar Spine Injury in Road Barrier Collision–Finite Element Study. Frontiers in Bioengineering and Biotechnology, **9**: 760498. doi: 10.3389/fbioe.2021.760498.

[45] Fields, A. J. (2010) Trabecular Microarchitecture, Endplate Failure, and the Biomechanics of Human Vertebral Fractures. PhD Thesis: University of California, Berkeley.

[46] Curry, W. H., Pintar, F. A., et al. (2016) Lumbar spine endplate fractures: Biomechanical evaluation and clinical considerations through experimental induction of injury. Journal of Orthopaedic Research, **34**(6): pp. 1084–1091. doi: 10.1002/jor.23112. Epub 2015 Dec 14. PMID: 26610067.

[47] Jäger, M. (2018) Extended compilation of autopsy-material measurements on lumbar ultimate compressive strength for deriving reference values in ergonomic work design: The Revised Dortmund Recommendations. EXCLI Journal, 17: pp. 362–385. doi: 10.17179/excli2018-1206. PMID: 29805345; PMCID: PMC5962898.

[48] Raftery, K. A., Kargarzadeh, A., Tavana, S., Newell, N. (2024) Disc degeneration influences the strain magnitude and stress distribution within the adjacent trabecular bone. Frontiers in Bioengineering and Biotechnology, **12**: 1511685. doi: 10.3389/fbioe.2024.1511685.

[49] Hussein, A. I., Louzeiro, D. T., Unnikrishnan, G. U., Morgan, E. F. (2018) Differences in Trabecular Microarchitecture and Simplified Boundary Conditions Limit the Accuracy of Quantitative Computed Tomography-Based Finite Element Models of Vertebral Failure. ASME. The Journal of Biomechanical Engineering, **140**(2): 021004. https://doi.org/10.1115/1.4038609.

[50] Mokhtarzadeh, H., Anderson, D. E., Allaire, B. T., Bouxsein, M. L. (2021) Patterns of Load-to-Strength Ratios Along the Spine in a Population-Based Cohort to Evaluate the Contribution of Spinal Loading to Vertebral Fractures. Journal of Bone and Mineral Research, **36**: pp. 704–711. https://doi.org/10.1002/jbmr.4222.

VIII. APPENDIX

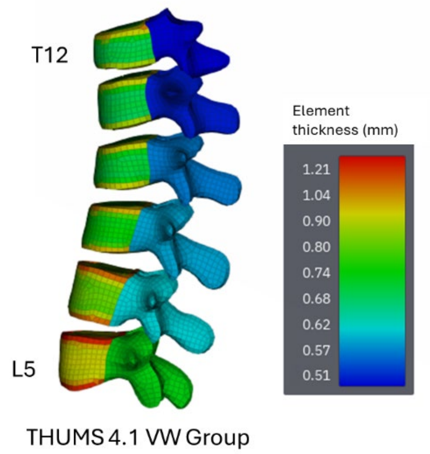

Fig. A1. Elementwise distribution of cortical thickness in modified THUMS 4.1 Group model lumbar vertebrae L5-T12.

TABLE AI
PMHS EXPERIMENT (ONLY MALE) DATABASE FOR 50TH PERCENTILE OCCUPANT VWG-HBM LUMBAR SPINE IRC DEVELOPMENT

S.No.	Ref.	Test	Age (yr)	Body mass (kg)	Stature (mm)	Loading Configuration	AIS2+ Injury Occured
1		1294	76	70	1780		
2		1295	47	68	1770		
3		1358	54	79	1770		
4		1359	49	76	1840		
5	[19]	1360	57	64	1750	Frontal sled test (40 km/h)	No Injury
6		1378	72	81	1840		
7		1379	40	88	1790		
8		1380	37	78	1800		
9		UVAS028	59	68	1780		
10		UVAS029	66	70	1790		
11		UVAS0302	67	68	1770	Frontal sled test (30 km/h)	
12		UVAS0303	67	68	1730		
13	[20]	UVAS0304	74	70	1830		No Injury
14		UVAS0313	69	69	1730		
15		UVAS0314	66	76	1715	Oblique sled test (30 km/h)	
16		UVAS0315	67	64	1765		
17		SubBIO_26	85	79	1650		Injury
18		SubBIO_27	84	57	1700	Front Seat (50 km/h)	Injury
19		SubBIO_28	84	64	1700		No Injury
20	[21]	SubBIO_29	89	77	1750		Injury
21		SubBIO_22	55	92	1770		No Injury
22		SubBIO_23	86	67	1680	Rear Seat (50 km/h)	Injury
23		SubBIO_24	87	77	1750		Injury
24		SubBIO_25	87	64	1710		No Injury
25	[22]	13119	71	53	1663	Frontal Sled Test (31.9 km/h)	No Injury
26		13109	80	80.3	1701	Frontal Sled Test (33 km/h)	No Injury

27		12796	72	80.7	1742	Frontal Sled Test (33.2 km/h)	No Injury
28	[22]	13124	70	63.7	1756	Frontal Sled Test (32.7 km/h)	No Injury
29		13110	85	71.1	1697	Frontal Sled Test (32.6 km/h)	No Injury
30		12795	91	76.1	1749	Frontal Sled Test (31.7 km/h)	No Injury
31	[23]	529	66	74	1750	Frontal Sled (50 km/h); 50° seat-back recline	Injury
32		530	53	57	1750		Injury
33		531	72	74	1850		Injury
34		532	25	75	1740		No Injury
35		533	55	74	1800		No Injury
36	[24]	Condition A Test 1	72±3.3	82.5±10.6	1776±64	Under-body blast Mild exposure: 4 m/s peak velocity with 5 ms time to peak on both floor and seat	No Injury
37		Condition A Test 2					No Injury
38		Condition A Test 3					No Injury
39		Condition A Test 4					Injury
40		Condition B Test 1				Under-body blast Moderate exposure: 4 m/s velocity with 10 ms TTP on the seat, 6 m/s velocity with 5 ms TTP on the floor	No Injury
41		Condition B Test 2					Injury
42		Condition C Test 1				Under-body blast Severe exposure: 6 m/s velocity with 10 ms TTP on the seat, 8 m/s velocity with 5 ms TTP on the floor	Injury
43	[25]	Test 1	57	67	1850	Inferior-Superior impact (6.09 ms/)	No Injury
44		Test 4	58	75	1820	Inferior-Superior impact (5.98 m/s)	No Injury
45		Test 6	63	58	1770	Inferior-Superior impact (2.84 m/s)	No Injury
46	[26]	PMHS 0701 Impact Location: Sacrum	60	81	1720	Loading due to Body Seal Closure during posterior landing Target Input : 10 g	No Injury
47		PMHS 0702 Impact Location: Sacrum	50	86	1840	Loading due to Body Seal Closure during posterior landing Target Input: 10 g	Interval Injury
48		PMHS 0702 Impact Location: Lumbar	50	86	1840	Loading due to Body Seal Closure during posterior landing Target Input: 20 g	
49		PMHS 0703 Impact Location: Sacrum	47	82	1750	Loading due to Body Seal Closure during posterior landing Target Input: 10 g	No Injury
50	[27]	Test 6	71	68.04	1780	Impact Velocity: 4.4 m/s	No Injury
51		Test 8	71	93.16	1715		No Injury
52		Test 11	62	51.71	1803		No Injury
53		Test 12	48	61.69	1721		No Injury
54		Test 13	47	64.49	1780		No Injury
55	[28]	UVA 516	89	54.4	1550	Impact Velocity: 3.08 m/s	No Injury
56		UVA 552	82	82	1700	Impact Velocity: 3.01 m/s	No Injury
57		UVA 631	71	71	1780	Impact Velocity: 3.63 m/s	No Injury
58		UVA 553	60	60	1700	Impact Velocity: 3.54 m/s	No Injury

59	[29]	HS75	65	61		Drop height: 0.9 m, Impact site: Vertex	No Injury
60		HS76	67	64		Drop height: 0.9 m, Impact site: Vertex	No Injury
61		HS77	82	66		Drop height: 0.9 m, Impact site: Occiput	No Injury
62		HS80	75	67		Drop height: 1.2 m, Impact site: Occiput	No Injury
63		HS81	73	83		Drop height: 1.2 m, Impact site: Occiput	No Injury
64		HS83	68	82		Drop height: 1.5 m, Impact site: Vertex	No Injury
65		HS84	71	64		Drop height: 1.5 m, Impact site: Vertex	No Injury
66	[30]	High Compression Test 236 (Segment : L1-L2)	43	72.2	1816	1.0 m/s	Injury
67		High Compression Test 276 (Segment : L1-L2)	46	80	1700		Injury
68		High Compression Test 286 (Segment : L1-L2)	54	79.4	1800		Injury
69		High Compression Test 306 (Segment : L1-L2)	60	75	1780		Injury
70		High Compression Test 326 (Segment : L1-L2)	52	74.9	1778		Injury
71		High Compression Test 346 (Segment : L1-L2)	56	95.3	1778		Injury
72		High Compression Test 156 (Segment : L2-L3)	45	96	1780		Injury
73		High Compression Test 186 (Segment : L2-L3)	60	98.1	1800		Injury
74		High Compression Test 216 (Segment : L2-L3)	41	74.5	1740		Injury
75		High Compression Test 246 (Segment : L2-L3)	59	58.1	1727		Injury
76		High Compression Test 226 (Segment : L3-L4)	43	72.2	1816		Injury
77		High Compression Test 266 (Segment : L3-L4)	46	80	1700		Injury
78		High Compression Test 296 (Segment : L3-L4)	60	75	1780		Injury
79		High Compression Test 316 (Segment : L3-L4)	54	79.4	1800		Injury
80		High Compression Test 336 (Segment : L3-L4)	56	95.3	1778		Injury

81		High Compression Test 366 (Segment : L3-L4)	51	77.3	1752		Injury
82		High Compression Test 146 (Segment : T12-L1)	45	96	1780		Injury
83		High Compression Test 166 (Segment : T12-L1)	60	98.1	1800		Injury
84		High Compression Test 206 (Segment : T12-L1)	41	74.5	1740		Injury
85		High Compression Test 256 (Segment : T12-L1)	59	58.1	1727		Injury
86		Low Compression Test 234 (Segment : L1-L2)	43	72.2	1816		No Injury
87		Low Compression Test 274 (Segment : L1-L2)	46	80	1700		No Injury
88		Low Compression Test 304 (Segment : L1-L2)	60	75	1780		No Injury
89		Low Compression Test 324 (Segment : L1-L2)	52	74.9	1778		No Injury
90		Low Compression Test 344 (Segment : L1-L2)	56	95.3	1778		No Injury
91		Low Compression Test 154 (Segment : L2-L3)	45	96	1780		No Injury
92		Low Compression Test 184 (Segment : L2-L3)	60	98.1	1800	0.5 m/s	No Injury
93		Low Compression Test 214 (Segment : L2-L3)	41	74.5	1740		No Injury
94		Low Compression Test 244 (Segment : L2-L3)	59	58.1	1727		No Injury
95		Low Compression Test 224 (Segment : L3-L4)	43	72.2	1816		No Injury
96		Low Compression Test 264 (Segment : L3-L4)	46	80	1700		No Injury
97		Low Compression Test 294 (Segment : L3-L4)	60	75	1780		No Injury
98		Low Compression Test 314 (Segment : L3-L4)	54	79.4	1800		No Injury
99		Low Compression Test 334 (Segment : L3-L4)	56	95.3	1778		No Injury

100		Low Compression Test 364 (Segment : L3-L4)	51	77.3	1752		No Injury
101		Low Compression Test 204 (Segment : T12-L1)	41	74.5	1740		No Injury
102		Low Compression Test 254 (Segment : T12-L1)	59	58.1	1727		No Injury
103	[31]	Segment : T12-L5	66	66.2		1 m/s	Injury
104		Segment : L1-L2	45	53			Injury
105		Segment : L2-L3	45	73.9			Injury
106		Segment : L3-L4	45	53			Injury
107		Segment : L4-L5	45	73.9			Injury
108	[32]	Drop Test S1.0, Specimen : HS530 (Segment : T12-L5)	45	100	1750		No Injury
109		Drop Test S1.0, Specimen : HS591 (Segment : T12-L5)	37	114	1800		No Injury
110		Drop Test S1.0, Specimen : HS657 (Segment : T12-L5)	26	100	1730		No Injury
111		Drop Test S1.0, Specimen : HS673 (Segment : T12-L5)	33	113	1880		No Injury
112	[33]	Ejection Catapult 1 (Segment :T12-L5)	42±13.7			Peak acceleration: 20.7 g; Rate of Onset: 228 g/s; Rise time: 91 ms	Injury
113		Ejection Catapult 2 (Segment : T12-L5)				Peak acceleration: 22.3 g; Rate of Onset: 513 g/s; Rise time: 44 ms	Injury
114		Helicopter Crash 1 (Segment : T12-L5)				Peak acceleration: 44.3 g; Rate of Onset: 1065 g/s; Rise time: 42 ms	Injury
115		Helicopter Crash 2 (Segment : T12-L5)				Peak acceleration: 64.9 g; Rate of Onset: 2638 g/s; Rise time: 25 ms	Injury
116		Helicopter Crash 3 (Segment : T12-L5)				Peak acceleration: 65 g; Rate of Onset: 2500 g/s; Rise time: 26 ms	Injury
117	[34]	Subject : 983 (Segment : T12 -L2)	63	93.9	1626	Compression force: 2200 N; Flexion 600 deg/sec	Injury
118		Subject : 938 (Segment : T12 -L2)	66	82.5	1676	Compression force: 3300 N; Flexion 600 deg/sec	Injury
119		Subject : 946 (Segment : T12 -L2)	41	99.8	1651	Compression force: 3300 N; Flexion 600 deg/sec	Injury
120		Subject : 985 (Segment : T12 -L2)	50	81.6	1854	Compression force: 4500 N; Flexion 600 deg/sec	Injury
121		Subject : 938 (Segment : L3-L5)	66	82.5	1676	Compression force: 3300 N; Flexion 600 deg/sec	Injury

122		Subject : 946 (Segment : L3-L5)	41	99.8	1651	Compression force: 4500 N; Flexion 600 deg/sec	Injury

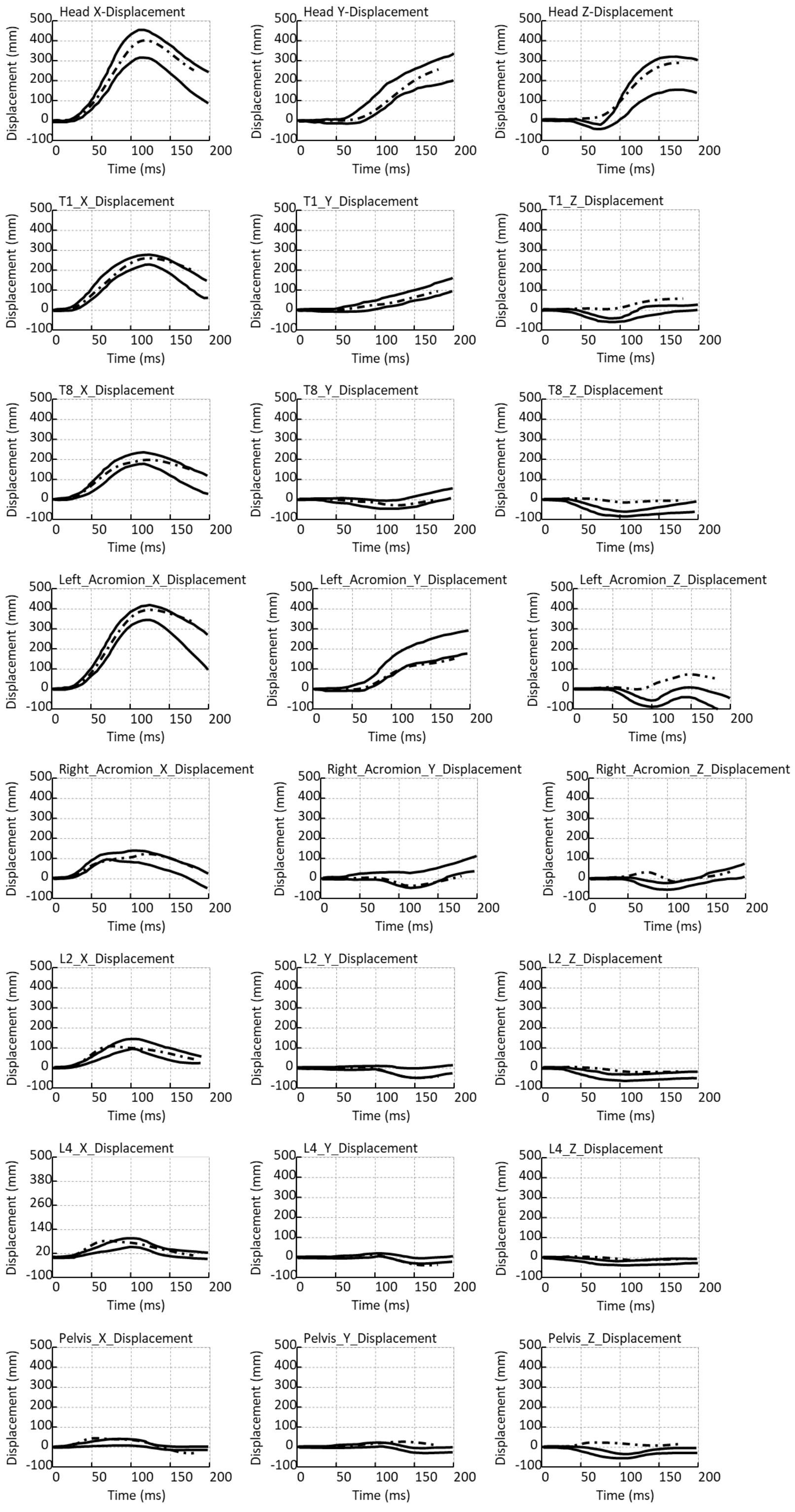

Fig. A2. 50th percentile male occupant VWG-HBM response (dash-dot line) for Shaw et al. (2009) load case. Solid lines indicate upper and lower boundaries (Ash et al. 2012).

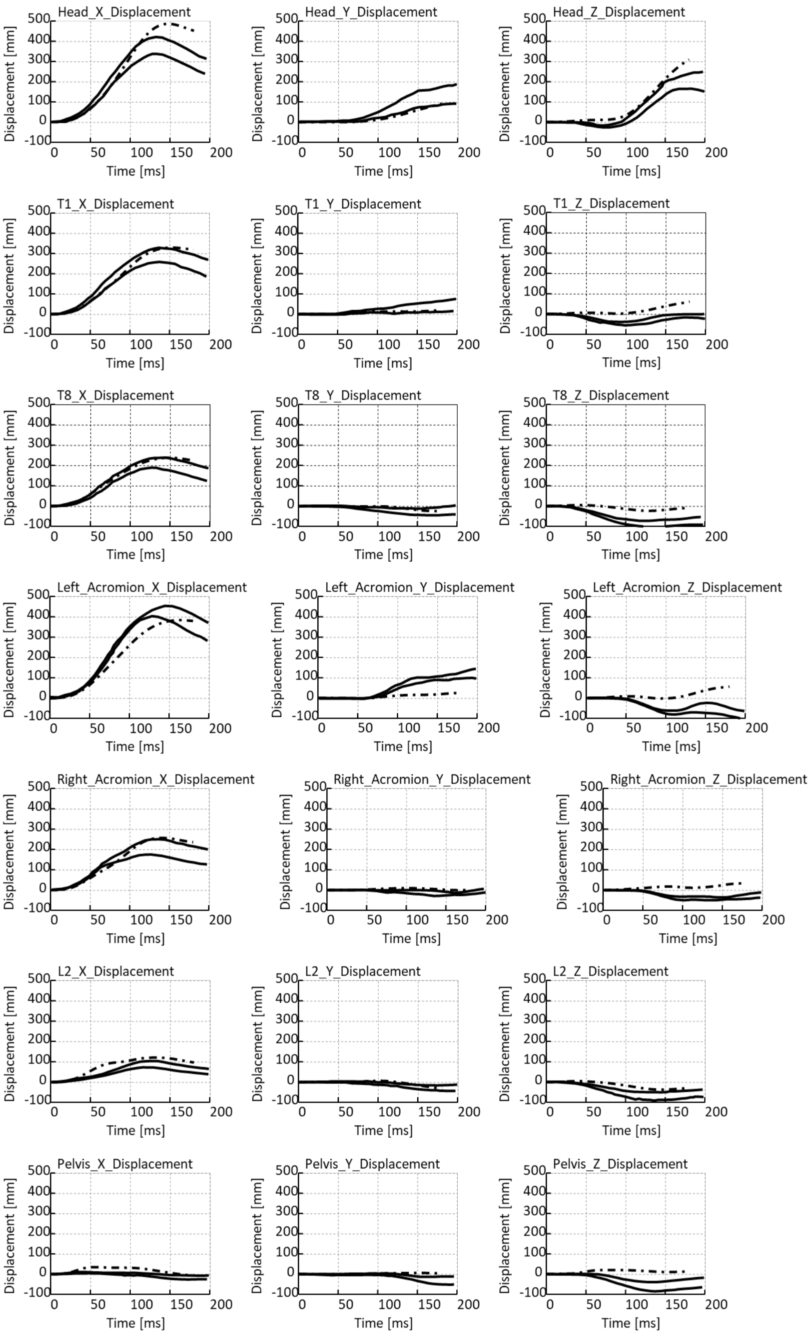

Fig. A3. 50th percentile male occupant VWG-HBM response (dash-dot line) for Acosta et al. (2009) frontal sled test. Solid lines indicate upper and lower boundaries.

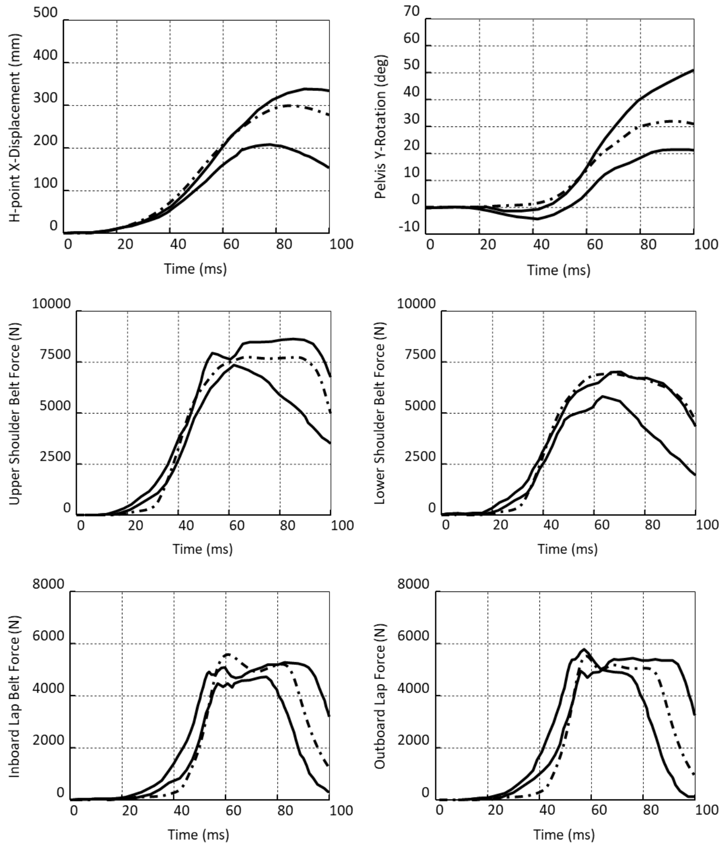

Fig. A4. 50th percentile male occupant VWG-HBM response (dash-dot line) for Uriot et al. (2015) front sled test. Solid lines indicate upper and lower boundaries.

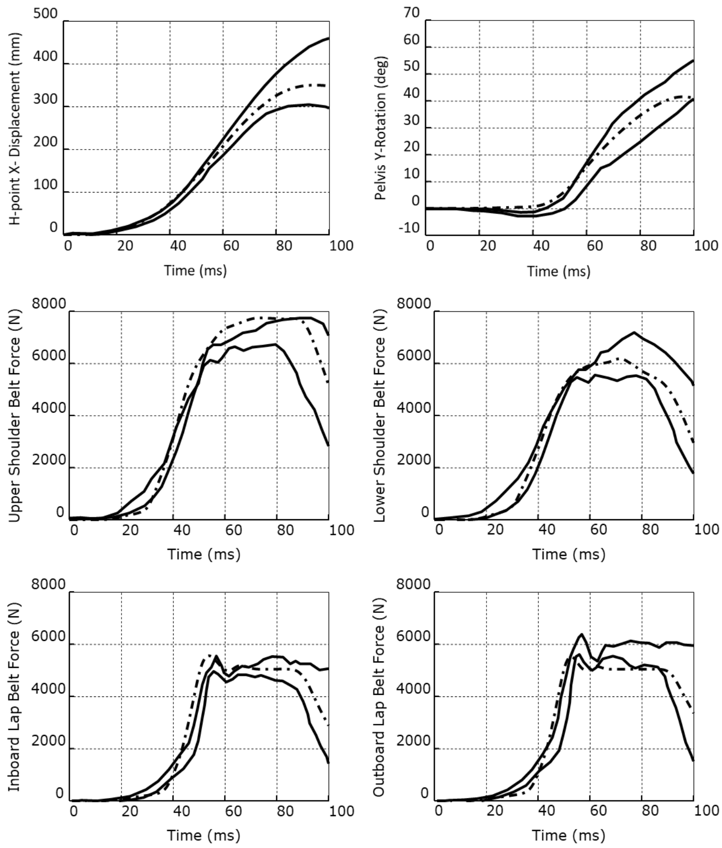

Fig. A5. 50th percentile male occupant VWG-HBM response (dash-dot line) for Uriot et al. (2015) rear sled test. Solid lines indicate upper and lower boundaries.

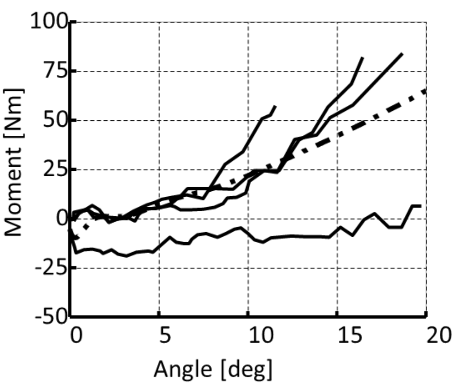

Fig. A6. 50th percentile male occupant VWG-HBM response (dash-dot line) for Tushak et al. (2022). Solid lines indicate upper and lower boundaries.